Measurement 196 (2022) 111221

Contents lists available at ScienceDirect

Measurement

journal homepage: www.elsevier.com/locate/measurement

Determination of stepped plate thickness distribution using guided waves and compressed sensing approach

Beata Zima

Faculty of Mechanical Engineering and Ship Technology, Gdańsk University of Technology, ul. Narutowicza 11/12, 80-233 Gdańsk, Poland

ARTICLE INFO

Keywords:
Guided waves
Plate structure
Variable thickness
NDT

ABSTRACT

Guided waves recently have attracted significant interest as a very promising research area. The signals registered by a specially designed sensor network are processed to assess the state of the tested structure. Despite the constant development of novel damage detection algorithms employing guided waves, the phenomenon of wave propagation still needs detailed recognizing and understanding for the further progress of non-destructive wave-based methods. Special attention is paid to guided waves in plate-like structures, but the majority of considered cases concern plates with constant thickness. However, in the real world, we often deal with specimens with variable thickness. The thickness variability of the specimen is often forced to fulfill the construction requirements and optimize stress distribution or is the result of degradation i.e. corrosion. Thus, the development of NDT methods forces the need of considering specimens with complex geometry and the problem of wave propagation in waveguides with variable thickness is crucial for improving novel as well as so far proposed algorithms.

The article presents the results of the analytical, numerical and experimental analysis of wave propagation in plates with variable thickness. The analysis concerns the influence of thickness distribution of plate structure on wave velocity, the time course wave packet and amplitude. Moreover, the novel approach based on constrained convex optimization for determining the plate thickness distribution has been proposed and verified during numerical and experimental campaigns.

1. Introduction

Guided waves have attracted significant research interest as means to conduct nondestructive inspections in a variety of structures [1–3]. Their potential for detection of relatively small damages impossible to detect during standard visual inspections has been demonstrated in many previous papers. Their ability to travel long distances without considerable amplitude decay makes them a suitable tool for diagnostics of long objects like pipes, rods, or rails.

The leading research centers in the world put an enormous effort into developing effective methods of nondestructive detection, localization, and sizing of the damage. In particular, wave-based SHM has focused considerable interest in the field of monitoring plate-like structures [4–8]. In many cases, the damage is localized based on the identification of reflection from the damage and determining the time lags between excited and registered waves. Next, the time of flight and the constant velocity determined from dispersion curves were used to localize the faulty region. The shape of dispersion curves strongly depends on plate thickness and material parameters, while the curves considered were determined for an undamaged, isotropic, homogeneous metal plate with constant thickness. The assumption about the uniform propagation path is one of the main limitations enabling the application of the so far developed methods in practice. One of the examples of damage requiring considering thickness variability is corrosion degradation. It is common damage to the vast majority of engineering structures, as well as the machines and their parts. The localized pits can occur simultaneously with general corrosion affecting not only the geometry of the specimen but also the metal microstructure. The assumption about isotropy and homogeneity may lead to inaccurate velocity determination and incorrect pits localization. Another recently analyzed examples are structures that, depending on the season and temperature, may be covered with additional non-uniform ice layers [9,10] or structures strengthened with tapered adhesive layers [11]. The local changes in wall thickness are common practice in aerospace or hull structures to fulfill the construction requirements and optimize stress distribution. The development of NDT methods in biomechanics [12] also forces the need of considering specimens with complex geometry. For this reason, the problem of wave propagation in tapered or non-uniform waveguides

E-mail address: beata.zima@pg.edu.pl.

https://doi.org/10.1016/j.measurement.2022.111221
Received 17 February 2022; Received in revised form 8 April 2022; Accepted 16 April 2022
Available online 20 April 2022

has been recently considered by researchers.

The theoretical analysis of Lamb wave propagation in a waveguide with varying heights was conducted by Pageneux and Maurel [13]. The technique of rearrangement of the equations of elasticity that provides a new system of coupled-mode equations preserving energy conservation was applied to the specimen with thickness described by the Gaussian function.

El-Kettani et al. [14] presented experimental and numerical results of adiabatic guided wave mode propagation in the plate with slowly linearly varying thickness. They proved that after reaching the thickness cut-off the adiabatic mode may reflect or convert into a different guided wave that propagates downslope in the plate. The mode conversion of shear horizontal guided wave mode in tapered plates was also observed by Nurmalia et al. [15]. Their conclusions were consistent with observations made by El-Kettani [14]: mode conversion of SH modes occurred when the thickness of the waveguide abruptly decreased to below the cut-off thickness. De Marchi et al. [16] developed a procedure to predict the group delay of stress waves propagating in tapered waveguides. They compared the predicted curves with those extracted from the time-frequency representation of simulated wave propagation in tapered waveguides. In [17] De Marchi et al. proposed the double-step method based on a warped frequency transform aimed at locating the damages in plates. Their algorithm has been validated and tested on irregular waveguides composed of uniform, tapered and curved segments. The evolution of the guided modes wavenumbers concerning position along the direction of propagation in the cortical bone-mimicking wedged plate was analyzed by Moreau et al. [18]. They adapted the singular value decomposition method usually used for plates with constant thickness to the case of waveguides of slowly linearly variable thickness. Moll et al. [19] analyzed the antisymmetric wave propagation in the tapered multilayered anisotropic structure and determined the thickness of particular segments using laser vibrometry and a terahertz time-domain system. In [20] Moll presented the damage localization technique taking into account the non-uniform nature of adiabatic wave motion in composite structures with smoothly varying thickness. Martinez et al. [21] demonstrated the damage detection procedure in plates with variable thickness based on the multi-frequency topological derivative. The numerical proof of concept was presented for varying numbers and arrangements of piezoelectric transducers mounted very close to the plate boundary. In their approach, the mode conversion associated with variable thickness and complex planform was naturally taken into account by using non-simplified elastodynamic equations instead of the Lamb propagation model.

Despite the enormous effort put into the detailed analysis of the wave propagation in waveguides with non-uniform thickness, there are still unsolved research gaps that demand consideration for the further development of the diagnostics methods. From the point of view of structural state evaluation, it is also important to estimate the minimum thickness of the non-uniform waveguide, which is critical for load carrying capacity or tightness of the whole structure. Thus, it is crucial to consider the inverse scattering problem dealing with the reconstruction of the plate shape based on the measured signals. To the authors' best knowledge, so far the dependency of irregular plate shape and signal characteristics, as well as the solution to the inverse problem of shape reconstruction has not been described in the literature, yet.

This article presents the theoretical, experimental, and numerical analysis of wave propagation in aluminum plates with non-uniform thickness. In the first stage, the influence of plate geometry on wave velocity, the shape i.e. time course of the incident wave, and its amplitude is analyzed. In the next stage, the attempt of solving the inverse scattering problem using the novel approach based on compressed sensing is presented. The influence of several measurements on the effectiveness of plate thickness variability reconstruction is analyzed. One of the greatest advantages of the proposed approach is the limited number of measurements and sensors attached to the structure. The stepped plate thickness reconstruction based on convex optimization requires knowledge only about the input and output signals measured at the ends of the plate.

The study indicates which signal parameters are dependent on thickness variability but are independent of exact plate shape. On the other hand, some parameters and their derivatives depend strongly on the exact specimen shape and they cannot be efficiently used in the thickness variability assessment. The results presented in the paper are crucial from the point of view of diagnostics of general degradation affecting plate geometry because they allow for the evaluation of which signal parameter can be efficiently used in the further development of dedicated damage indexes.

2. Theoretical background

2.1. The influence of geometry on wave propagation velocity

Guided waves are dispersive waves, which means that their velocity depends on excitation frequency. The well-known relation between velocity and frequency is described by dispersion equations formulated by Lamb in 1917 [1], [22]:

$$\frac{\tan(qd)}{\tan(pd)} = -\frac{\left(k^2-q^2\right)^2}{4k^2pq} \tag{1}$$

$$\frac{\tan(qd)}{\tan(pd)} = -\frac{4k^2pq}{\left(k^2-q^2\right)^2} \tag{2}$$

The parameters d and k indicate the plate thickness and the wavenumber, respectively. Parameters q and p depend on longitudinal and transverse wave velocities.

The plate thickness d is one of the parameters occurring in Lamb equations. Thus, every thickness change involves a change in propagation velocity. Let's assume that the plate is divided into n divisions with a length Δx. The time needed to travel the distance Δx is equal to:

$$\Delta t_i = \frac{\Delta x_i}{c_{g_i}} \tag{3}$$

The total time of flight along the distance L is a sum of the particular times of flight along with the distances Δx:

$$ToF = \sum_{i=1}^{n} t_i = \sum_{i=1}^{n} \frac{\Delta x}{c_{g_i}} = \Delta x \sum_{i=1}^{n} \frac{1}{c_{g_i}} \tag{4}$$

The average wave velocity is then described by the equation:

$$c_{g,mean} = \frac{L}{ToF} = \frac{L}{\Delta x \sum_{i=1}^{n} \frac{1}{c_{g_i}}} = \frac{n}{\sum_{i=1}^{n} \frac{1}{c_{g_i}}} \tag{5}$$

Based on the above equation one can conclude that the exact shape of the plate surface does not influence the average wave velocity along the propagation path L. The average wave velocity is influenced only by the thickness distribution, which means that two plates varying in shape can be characterized by the same wave velocity. The equation is valid for all excitation frequencies, so for other parameters of the input excitation, we will get the same results for various plates. Thus, the wave velocity cannot be used as an indicative parameter in exact plate shape reconstruction but can be used in thickness distribution determination.

2.2. The influence of plate geometry on wave packet shape

The time variability of the propagating waveform $u(x,t)$ depends on the distance from the excitation point and the dispersion frequency-wavenumber dependency. The following form of the basic Dispersion Compensation Method equation is known:

$$u(x,t) = \int_{-\infty}^{\infty} F(\omega) e^{i(\omega t - k(\omega)x)} d\omega \tag{6}$$

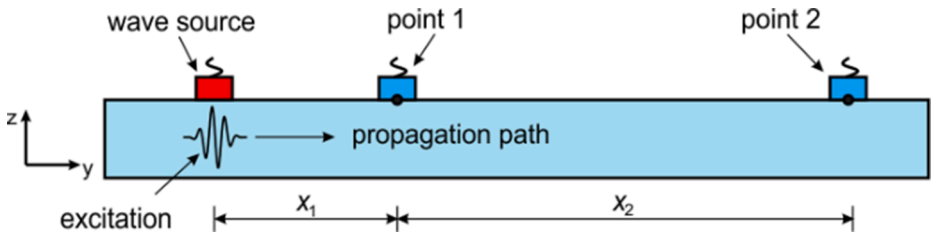

Fig. 1. Wave propagation in plate: excitation by the actuator and registration in points 1 and 2.

where $F(\omega)$ describes the frequency spectrum of excitation function while x denotes the distance from the wave source. To take into account the amplitude decay related to dispersion effects as well as the increasing distance from the source, the additional multiplying factor has to be introduced in the equation [23]:

$$u(x,t) = \frac{e^{-\xi x}}{\sqrt{2\pi x}} \int_{-\infty}^{\infty} F(\omega) e^{i(\omega t - k(\omega)x)} d\omega \tag{7}$$

For the sake of simplicity, the exponential factor will be denoted as $A(x)$. Then, Eq. (10) can be rewritten as follows:

$$u(x,t) = A(x) \int_{-\infty}^{\infty} F(\omega) e^{i(\omega t - k(\omega)x)} d\omega \tag{8}$$

The same equation can be also rewritten in the frequency domain:

$$\begin{aligned} U(x,\omega) &= U(0,\omega)H(x,\omega) \\ H(x,\omega) &= A(x,\omega)e^{-iK(\omega)x} \end{aligned} \tag{9}$$

where ω is the angular frequency and $U(x,\omega)$ and $U(0,\omega)$ are the frequency spectra of the signal $u(x,t)$ and excitation function $u(0,t)$. $H(x,\omega)$ denotes the transfer function, where $K(\omega)$ represents the nonlinear relation between wavenumber and the frequency. Because the amplitude variability in the frequency domain is not defined and in this section, only the shape of the propagating wave is considered, the factor $A(x,\omega)$ will be omitted in the following derivations by assuming that $A(x,\omega) = 1$. The amplitude variability will be considered in the next section.

Based on the above equations we can write the expression describing the signal at point 1 located at distance x_1 from the source (Fig. 1):

$$U(x_1,\omega) = U(0,\omega)e^{-iK_1(\omega)x_1} \tag{10}$$

Now, let's the signal registered in point x_1 can be treated as an excitation function and we can write the equation describing the signal in point 2 located at the distance x_2 from point 1:

$$U(x_2,\omega) = U(x_1,\omega)e^{-iK_2(\omega)x_2} \tag{11}$$

By substituting Eq. (13) into Eq. (14) we obtain:

$$U(x_2,\omega) = U(0,\omega)e^{-iK_1(\omega)x_1}e^{-iK_2(\omega)x_2} = U(0,\omega)e^{-i(K_1(\omega)x_1 + iK_2(\omega)x_2)} \tag{12}$$

The above equation can be rewritten in the more general form for the plate with variable thickness:

$$U(x_n,\omega) = U(0,\omega)e^{-i(\sum_{i=1}^{n} K_j(\omega)x_j)} \tag{13}$$

Based on the above derivations one can conclude that the shape of the wave packet depends on the thickness distribution along the propagation path but not on the exact shape of the plate. The time course depends on the frequency spectrum of the excitation $U(0,\omega)$ and the sum of the products of the distances and corresponding wavenumbers $K(\omega)x$ depending on the actual plate thickness.

2.3. The influence of plate geometry on wave amplitude

It is easy to prove that equations defined in the previous section cannot be directly transferred for amplitude calculation. From Eq. (14) we would obtain that:

$$A(x_1 + x_2, \omega) = A(x_1,\omega)A(x_2,\omega) \tag{14}$$

which is not true:

$$\frac{e^{-\xi x_1}}{\sqrt{2\pi x_1}} \frac{e^{-\xi(x_2 - x_1)}}{\sqrt{2\pi(x_2 - x_1)}} \neq \frac{e^{-\xi x_2}}{\sqrt{2\pi x_2}} \tag{15}$$

Moreover, the above expression was proposed based on the phenomenological model and despite it correctly predicts the exponential amplitude decay, still no instructions on how to set the damping parameter ξ have been proposed. The dispersion property of guided waves and energy conservation cause different frequency components propagate with a different velocity which results in spreading the wave packet and decreasing the amplitude. Thus, the amplitude decay may not depend only on the distance from the source but also on the parameters of the excitation.

Practically, it is difficult to compare the amplitude measured for different specimens, because it can be also influenced by the method of transducers attachment. Thus, in the following study, the amplitude variability is analyzed mainly numerically.

The derivations presented in the following Section indicate that the average wave velocity can be used only as an indicative parameter in plate thickness distribution, but because it does not depend on the geometry, it cannot be used for exact shape reconstruction. A similar observation was made for the shape of the wave packet: it depends on thickness distribution but not on the specific geometry. On the contrary, the amplitude value depends on the geometry and it varies for specimens with the same thickness distribution but different geometry. One can conclude that the amplitude value would be not an efficient indicative parameter in, for example, global damage assessment (like corrosion) leading to changes in all specimen geometry because two objects with the same degree of degradation would be characterized by different

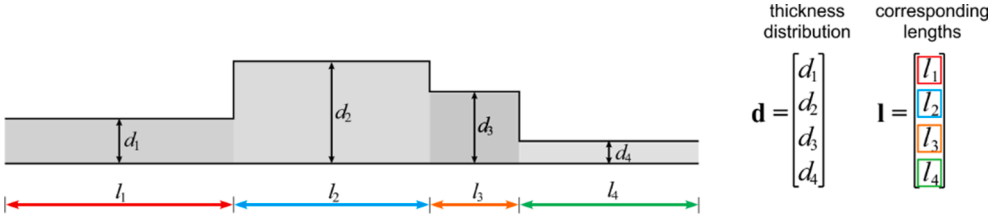

Fig. 2. Stepped plate and its thickness distribution.

amplitudes, but on the other hand, the amplitude can be potentially used in shape reconstruction, as it is the only sensitive parameter in this case.

The correctness of the derivations presented above was verified during experimental and numerical investigations and is presented in the further part of the paper.

3. Determination of thickness distribution of plate structure using CS approach

This section contains the description of the novel approach to thickness distribution of the stepped plates. The thickness distribution of any plate along the propagation path can be described by two vectors. The first vector $\boldsymbol{d} = \{d_1, d_2, ..., d_n\}^T$ contains the thickness values, while the second vector $\boldsymbol{l} = \{l_1, l_2..., l_n\}^T$ contains the distances corresponding to certain thicknesses (Fig. 2).

Let's define now the dictionary matrix $\boldsymbol{\Phi}$, which contains the reciprocals of the group velocity c_g:

$$\boldsymbol{\Phi} = \begin{bmatrix} \frac{1}{c_g^{f_1,d_1}} & \cdots & \frac{1}{c_g^{f_1,d_n}} \\ \vdots & \ddots & \vdots \\ \frac{1}{c_g^{f_m,d_1}} & \cdots & \frac{1}{c_g^{f_m,d_n}} \end{bmatrix} \tag{16}$$

Each column is associated with one thickness, while each row corresponds to one excitation frequency. Based on the derivations presented in Section 3.1 we can formulate the following equation:

$$\boldsymbol{\Phi l} = \boldsymbol{t} \tag{17}$$

where vector **t** contains the times of flight calculated for the particular frequencies propagating along with the plate with variable thickness. The dictionary matrix can be determined based on theoretical or numerical analysis, as well as may contain the experimental measurements. Vector **t** is the result of the experimental tests. The only unknown in the above equation is the vector **l** describing plate thickness variability. Unfortunately, the solution to the above problem is not straightforward, because the matrix **Φ** does not have to be square. In such a case it cannot be easily inverted. If the number of unknowns is greater than the number of equations, which is the common case, especially if the thickness reconstruction has to be accurate, then Eq. (20) describes the underdetermined system of equations with an infinite number of possible solutions. The solution to this problem can be achieved using a sparsity-promoting optimization technique. It is easy to notice that in the case of the stepped plate the vast majority of elements in vector **l** will be equal to zero and thus, the vector **l** can be considered sparse in the thickness domain. Once the compressed sensing problem is formulated, we can add the additional conditions, which must be set. The recovery of the plate thickness distribution is conducted by searching for the sparsest coefficient vector **l**, which agrees with the time of flight measurements, which can be presented by the following formulation:

$$\min_{\boldsymbol{l}} \|\boldsymbol{l}\|_0 \text{ such that } \boldsymbol{\Phi l} = \boldsymbol{t} \tag{18}$$

where ℓ_o norm $\|\boldsymbol{l}\|_0$ is the number of non-zero elements in vector **l**. Unfortunately, Eq. (21) is non-convex and represents NP-hard ill-posed inverse problem [24]. Based on the compressed sensing theory the solution can be efficiently approximated by minimizing ℓ_1 norm, which is the sum of non-zero entities in vector **l**:

$$\min_{\boldsymbol{l}} \|\boldsymbol{l}\|_1 \text{ such that } \boldsymbol{\Phi l} = \boldsymbol{t} \tag{19}$$

Furthermore, if the possible inaccuracies in time of flight determination are taken into account, Eq. (22) can be rewritten as [25]:

$$\min_{\boldsymbol{l}} \|\boldsymbol{l}\|_1 \text{ such that } |\boldsymbol{\Phi l} - \boldsymbol{t}| < \varepsilon \tag{20}$$

where ε is the inaccuracy level. We additionally know that all elements of vector **l** have physical meaning. They represent the distances with the same thickness and therefore every element must be positive. Moreover, their sum must be equal to the total distance L between the excitation and registration point. The final set of equations that have to be solved can be presented in the following form:

$$\begin{cases} \min_{\boldsymbol{l}} \|\boldsymbol{l}\|_1 \text{ such that } |\boldsymbol{\Phi l} - \boldsymbol{t}| < \varepsilon \\ \min \boldsymbol{l} \geqslant 0 \\ \sum_{i=1} l_i = L \end{cases} \tag{21}$$

The above description already demonstrated the possible advantages of the proposed CS-based approach. First of all, it does not require extensive measurements. Usually, the detailed mapping of the structure requires using laser vibrometry and capturing the signals on the plate surface. The CS-based approach requires using the network comprised of two transducers attached at the ends of the propagation path. Moreover, the proposed procedure does not demand extensive signal processing: the only parameter extracted from captured signals is the time of flight. The last advantage of the novel method is the lack of assumption about the constant plate thickness. The assumption that the non-uniform thickness can be approximated by the averaged thickness is not applied here.

Despite the above advantages, the possible drawbacks of the CS-based method must be mentioned here. First of all, the proposed method requires a dictionary matrix containing the information about determined parameter dependent on plate thickness. In this case wave velocity is considered, which can be determined using dispersion relations. However, usually, the experimental measurements are affected by some inaccuracies, which in turn influence the reconstruction of thickness distribution. The possible solution would be the experimentally determined dictionary matrix but the measurements made on plates with various thicknesses are not always possible. Thus, the accuracy of the developed approach based on an analytically determined matrix and experimental measurements will be tested in the next section (see Section 5.4).

The next limitation is the fact that the thickness distribution is investigated only alongside the propagation path between actuator and sensor. If the plate has an irregular surface cause i.e. by general degradation, the thickness reconstruction obtained using one pair actuator-sensor should be considered only as rough information. The detailed mapping probably would demand a more extensive transducers network (but still the number of processed signals would be smaller than in the case of scanning by laser).

The correctness of the proposed CS-based approach will be analyzed numerically and experimentally. The results presented in the further part of the paper faithfully demonstrate both advantages and disadvantages mentioned above.

4. Materials and methods

4.1. Numerical simulation

Numerical simulations of guided wave propagation in the stepped plate were conducted in the commercial FEM-based program Abaqus. The numerical models were developed using eight-node brick finite elements with reduced integration (C3D8R). The size of the elements was adjusted based on the mesh convergence study. The dimensions of the elements were the same and were equal to 1 mm × 1 mm. The transient wave propagation problem was solved with the integration time step equal to 10^{-7} s. The excitation was applied as a concentrated force in the middle at the edge of the plate. The wave excitation performance was conducted by applying a five-cycle sine function modulated by the Hanning window. The plate material was elastic and isotropic. Both, material parameters and the employed frequency range were set based

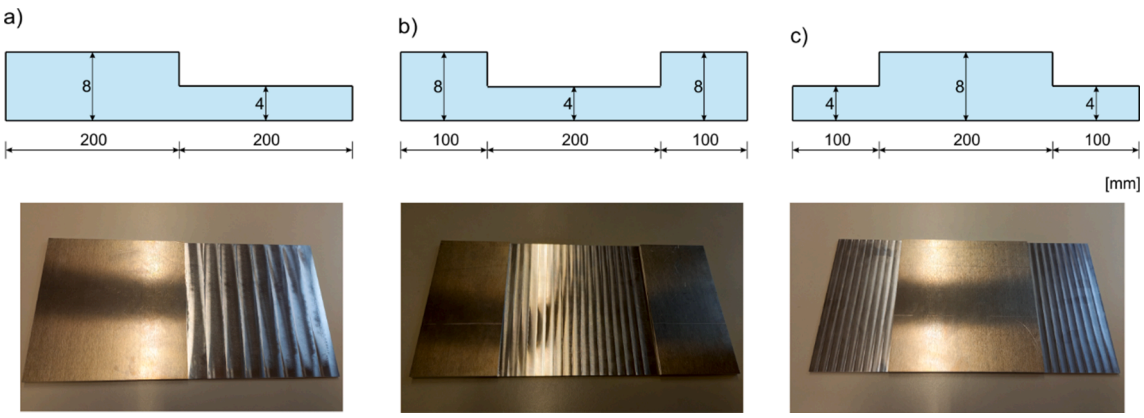

Fig. 3. Geometry of tested specimens a) plate #1, b) plate #2 and c) plate #3.

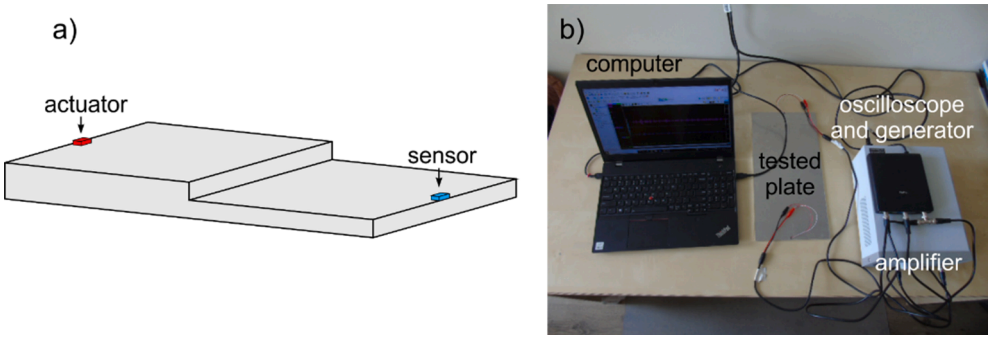

Fig. 4. Experimental setup: a) configuration of the transducers and b) used instrumentation.

on the experimental data. The numerical simulations and experimental tests were conducted for three cases described in the next section.

4.2. Experimental models

Experimental tests were conducted for three aluminum plates varying in shape but with the same material parameters (elastic modulus $E = 70$ GPa, density $\rho = 2700$ kg/m^3, Poisson's ratio $\nu = 0.33$). The geometry of the tapered plates is presented in Fig. 3. As we can see, the thickness distribution of the plates is exactly the same (the half of the plate has 8 mm, and the second half has 4 mm) but their shapes are different. The length of the plates was 400 mm, while the was 200 mm.

4.3. Experimental procedure

In the experimental tests, guided waves were propagated along with the tapered plates. Guided waves were excited and registered by using the oscilloscope, amplifier function generator connected with rectangular transducers attached by glue in the middle points at both ends of each plate (Fig. 4). The excitation was in the form of ten cycle sine modulated by the Hanning window. The carrier frequency was equal from 50 kHz to 150 kHz with a step of 10 kHz. In total, 16 carriers were used.

5. Results

5.1. Numerical results – The influence of thickness variability on wave velocity and packet shape

In the first step, the results for plates #1, #2 and #3 (see Fig. 3) for various excitation frequencies (50, 100 and 150 kHz) were collected and compared in Fig. 5. In the left column, time-domain signals registered at the plate end after excitation at the opposite end are presented. In each case, the initial part of the signal containing the incident wave has been highlighted by a grey color. Regardless of the various geometries of all three plate models, the time course of the initial part of the signal is exactly the same, which stays in agreement with derivations presented in Section 2.2. In the case of higher frequencies 100 and 150 kHz (Fig. 5b and c, respectively) because of wave overlapping it was impossible to extract only incident waves and thus not only the first incident wave was highlighted. However, the shape even of the following wave packets remained the same.

In the remaining time range, the signals for particular plates are different, but the differences are caused by the presence of reflections from edges and waves triggered in the "fault line".

The right column contains signal envelopes plotted using the Hilbert transform. The first peak of each signal was marked by a black dot to indicate that the time of flight of the first arriving waves is also the same. As previously, in the case of higher frequencies, namely 100 and 150 kHz, the times of flight of the two first peaks were indicated in the figure, to demonstrate that the equality of average velocities affects both antisymmetric and symmetric modes, which could be triggered by the irregularities in geometry. Wave velocity of antisymmetric modes is used in the further part of the paper to determine the thickness distribution.

5.2. Numerical results – the influence of thickness variability on signal amplitude

The last analyzed parameter is the amplitude. As derived, it is strongly dependent on the plate shape. The notably lowest amplitude is observed in the case of plate #2. One can say that the more intense amplitude decay in the case of plate #2 is associated with the double change of the cross-section, which in turn results in wave diffractions,

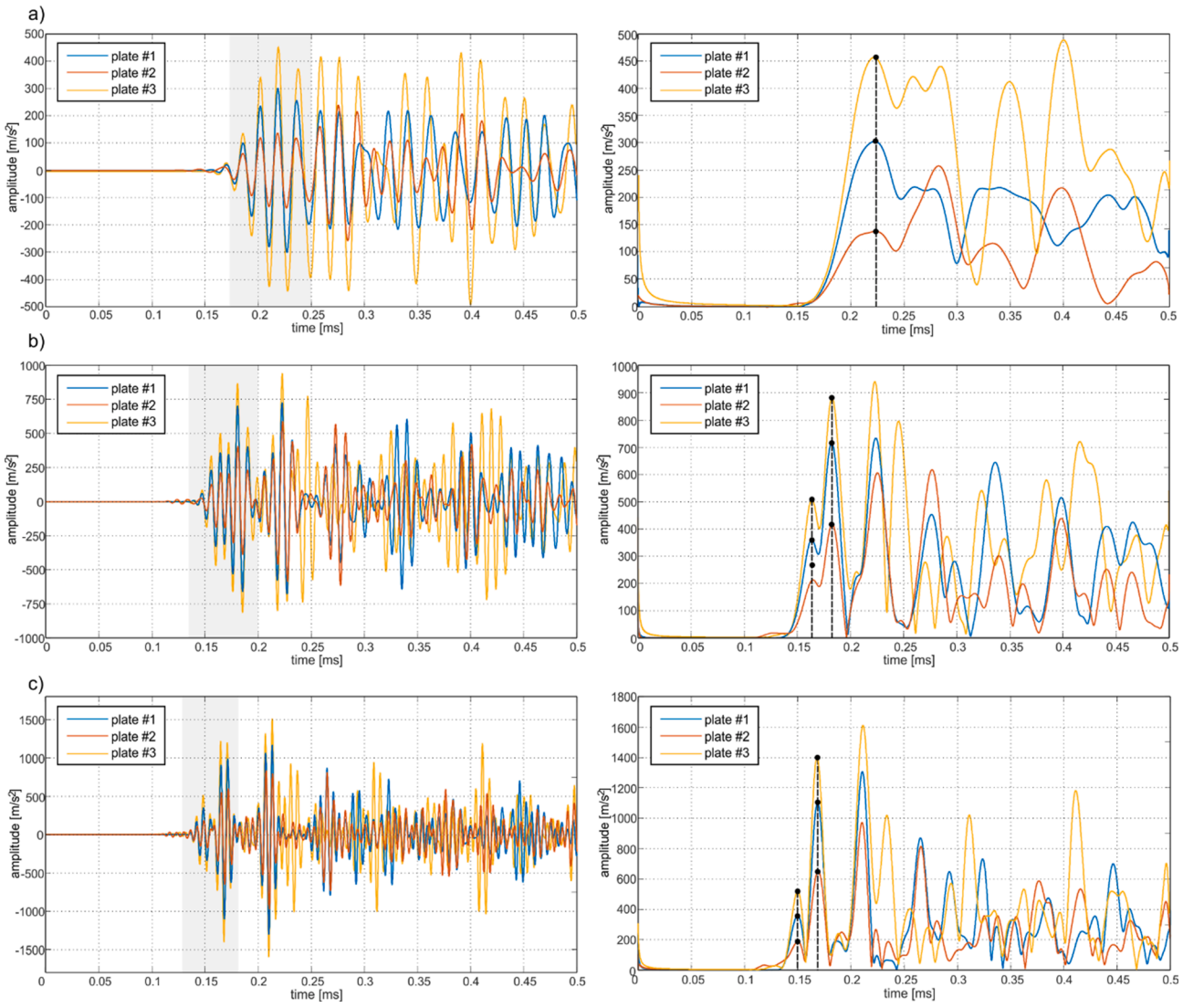

Fig. 5. Numerical signals and their envelopes obtained for plates #1, #2 and 3# for frequency of a) 50 kHz, b) 100 kHz, and c) 150 kHz.

mode conversions, and dissipation of a higher amount of energy. However, the highest amplitude was registered for plate #3 also with a double change of the cross-section.

To analyze the impact of thickness variability on wave amplitude the peak values along the propagation paths representing the distance-amplitude relationship were collected in Fig. 6. The signals were registered in each node lying on the propagation path and next the maximum value of the envelope of the incident wave was extracted. For comparison, the curves determined for plates with a constant thickness of 4 and 8 mm were additionally depicted.

When the wave is excited in the plate with a thickness of 4 mm (Fig. 6b and d) the curve coincides perfectly with the curve traced for the plate with a constant thickness of 4 mm but when the cross-section changes and the thickness increases we observe the sudden drop of the curve. However, after the amplitude decrease, the curve does not coincide with the curve traced for the plate with a constant thickness of 8 mm and the amplitude is higher than predicted. The situation is symmetric for results presented in Fig. 6a and c. After initial concurrence of the curves for plate with variable thickness and plate with a constant thickness of 8 mm, the amplitude increase is observed when the plate thickness decreases. After amplitude amplification, the curve does not coincide with the curve for 4 mm and is significantly lower. These changes, which were indicated in the figure by dashed vertical lines, can be explained by the decreasing or increasing volume in which the wave spreads. But the amplitude increase associated with the reduction of plate thickness is significantly less observable than the amplitude drop caused by thickness increase. The effect of amplitude decreasing and increasing is clearly visible in the visualization of wave propagation presented in selected time instants (Fig. 7). The visualization was performed for plates #1 and 3# for comparison and in the case of plate#1 additionally, both configurations of actuator and sensor were considered.

The first snapshots illustrate wave excitation ($t = 0.0035$ ms) in all three cases. In the second snapshot, we can see the wave interaction with the fault line. Because of differences in wave propagation velocity and in plate geometry, the visualizations were performed for different time instants in this case. To observe the differences in wave amplitude, we used the cut view and zoomed the fault line region. In the first and third case (Fig. 7a, $t = 0.105$ ms and Fig. 7c, $t = 0.06$ ms) we can observe wave propagation from the thinner part to the thicker part, which is associated with an amplitude decrease visible in visualization. The thinner the plate is more susceptible to deformation and if we assume that propagating wave is characterized by a certain amount of energy transferred from point to point, one can conclude that the deformations caused by wave motion should be smaller in plates with greater thickness. The same effect is also observable for the subsequent reflections i.e. in

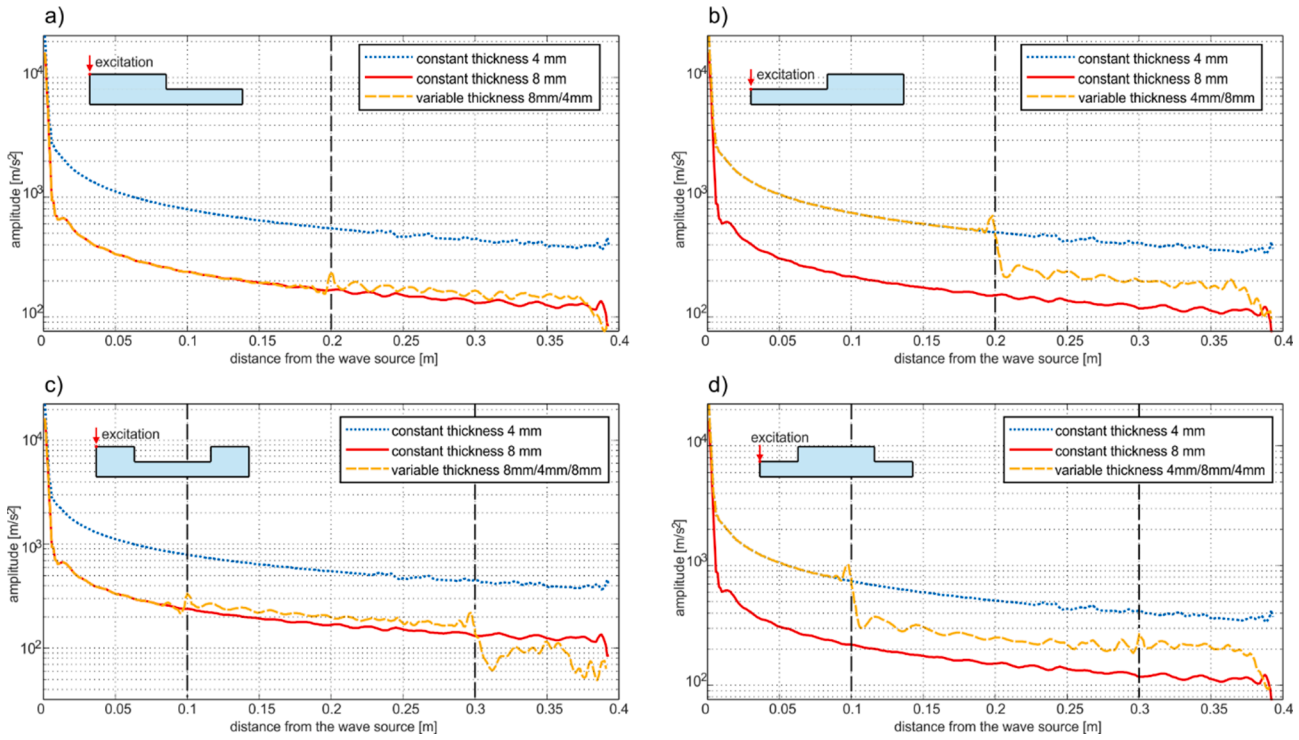

Fig. 6. Amplitude of propagating incident wave registered at different distances from the source in a) plate #1, b) plate #1 (reversed configuration of actuator and sensor), c) plate #2 and d) plate #3.

Fig. 7a, $t = 0.115$ ms.

The opposite situation takes place in cases presented in Fig. 7b, $t = 0.105$ ms and Fig. 7c, $t = 0.135$ ms. Propagation from thicker to thinner part is related to amplitude increase but it is less visible than amplitude decrease. The explanation might be the disruption of energy transfer through the "fault line". The part of wave energy is reflected from the perpendicular surface and propagates back alongside the plate (Fig. 7b, $t = 0.14$ ms).

Thus, one can conclude that the problem is not straightforward and the amplitude change is not linearly dependent on the plate thickness. The sequence of amplitude decreasing and increasing caused by thickness variability occurring at different distances from the source makes the issue of its prediction very complex.

5.3. *Numerical determination of plate thickness distribution*

In the next stage, the possibility of determining plate thickness variability using the convex optimization method described in Section 3 was investigated. To avoid additional inaccuracies, the dictionary matrix was created based on numerical results. It contains the velocity reciprocals for thickness varying from 1 mm to 20 mm with a step of 1 mm and for frequencies from 50 kHz to 150 kHz with a step of 10 kHz. The method of tracing the numerical dispersion curves using FFT has been described in detail in [26,27].

Because the time of flight was independent of the plate shape, the vector $\mathbf{t}$ was the same in all cases and thus the resulting vector $\mathbf{l}$ has also the same representation. The numerically obtained thickness distribution is presented in Fig. 8. Vector $\mathbf{l}$ contained only two non-zero elements corresponding to thicknesses of 4 and 8 mm. Both lengths were equal to 20 cm, which perfectly fits the geometry of the performed models.

In Fig. 9 the thickness distributions for various formulations of dictionary matrix have been collected. The solutions in Fig. 7a and b have been obtained based on the limited number of measurements, while the dictionary matrix was not modified. In the first step (Fig. 9a) the measurements were made for frequencies from 50 kHz to 150 kHz with a step of 20 kHz. Thus, the size of the dictionary matrix and vector $\mathbf{t}$ was twice smaller than previously. The solution in Fig. 9b has been obtained for measurements made only for three frequencies: 50, 100 and 150 kHz. According to the obtained solutions, the longest parts of the plates are characterized by the thickness of 4 and 7 mm, and 4 and 6 mm, respectively. It would be considered a good approximation of the exact thickness distribution but in both cases also other elements of vector $\mathbf{l}$ are non-zero and the solutions are less sparse and more complex than the actual plate shape.

The next two graphs present the solutions obtained for the limited number of considered thicknesses in the dictionary matrix. The measurements were made for frequency from 50 to 150 kHz with a step of 10 kHz, but the plate thickness varied from 2 mm to 20 mm with a step 2 mm (Fig. 9c), or from 4 mm to 20 mm with a step 4 mm (Fig. 9d). The vectors were more sparse than previously, but it should be noted that the possible solution range was significantly limited. Even though the distribution in Fig. 9d corresponds to the actual model shape, it was "forced" by the conditions set for the resulting vector $\mathbf{l}$.

The obtained results indicate that the reconstruction of the thickness distribution of tapered or stepped plates based on wave velocity and constrained convex optimization method is possible and it requires the proper construction of a dictionary matrix. In the case of a very limited number of measurements, the representation of vector $\mathbf{l}$ does not correspond to the actual plate shape. However, as already mentioned the particularly important parameter is the minimal plate thickness, which has been predicted with a very high agreement in every case.

5.4. *Experimental results - the influence of thickness variability on wave velocity and packet shape*

The experimental comparison presented in Fig. 10 with the FEM equivalent in Fig. 5 leads to the following observations. Firstly, the equality of the time of flight and the shape of the wave packets representing antisymmetric modes are observable in each case. Also, the time of flight of triggered symmetric modes is the same, which proves the correctness of the theoretical derivations which states that the time of flight and time representation of propagating wave does not depend on

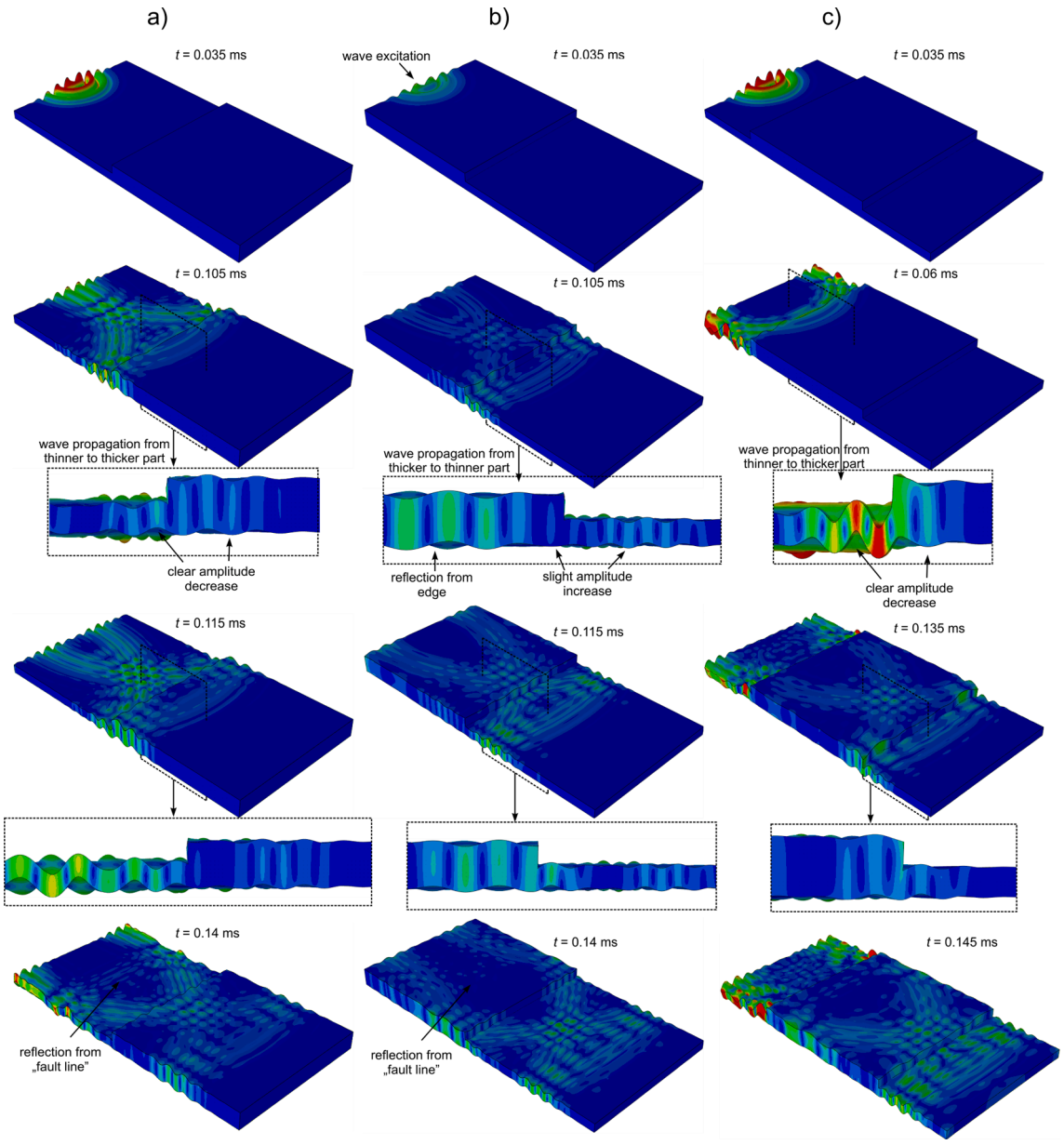

Fig. 7. Visualization of wave propagation in plate #1 a) after excitation at the thicker part and) after excitation at the thinner part and c) in the plate #3.

the exact plate shape but only on thickness distribution. Fig. 10 depicts the results only for three cases (50, 100 and 150 kHz) but a similar observation was made also for other excitation frequencies.

Secondly, the shapes of symmetric mode registered for 100 kHz are not perfectly the same and also the time range within the signals for various plates overlap is shorter than in the case of numerical signals. However, this may be the result of material and geometric imperfections or imperfect sensor attachment which do not occur in numerical models.

Thirdly, for the same frequencies, significant differences in amplitudes are observed. As in the case of numerical studies, the lowest amplitude was noted for plate #2 and the highest for plate #3 which stays in agreement with numerical results.

5.5. *Experimental determination of plate thickness distribution*

The thickness reconstruction was proceeded by creating the dictionary matrix. As mentioned, the matrix can be created using analytical, numerical, or experimental data. However, in the case of the experimentally determined matrix, the following studies would require the measurements conducted on twenty aluminum plates with various thicknesses. Therefore, in the first step the dictionary was created based on the solution of the dispersion Lamb equation (see Eq. (1) and (2)).

The experimental velocities usually do not coincide perfectly with the analytical curve so to estimate the possible inaccuracies in time of flight determination and the value of the parameter ε, the measurements were first carried out on plates with a constant thickness of 4 and 8 mm (Fig. 11). For comparison, the analytically determined dispersion curves were added in the figure. The slight deviations between theoretical and analytical results might lead to inaccuracies in plate thickness reconstruction which is the main limitation of the proposed method (see Fig. 12).

The results of the thickness reconstruction based on an analytically determined dictionary matrix are presented in Fig. 13. As previously, because the times of flights for all plates were the same, the results in the form of thickness distribution were also the same. For clarity and to avoid duplication, the article contains only one set of results. The maximal length corresponds to a thickness of 6 mm (34.17 cm). The nonzero lengths were obtained also for thicknesses 4 mm (5.14 cm) and

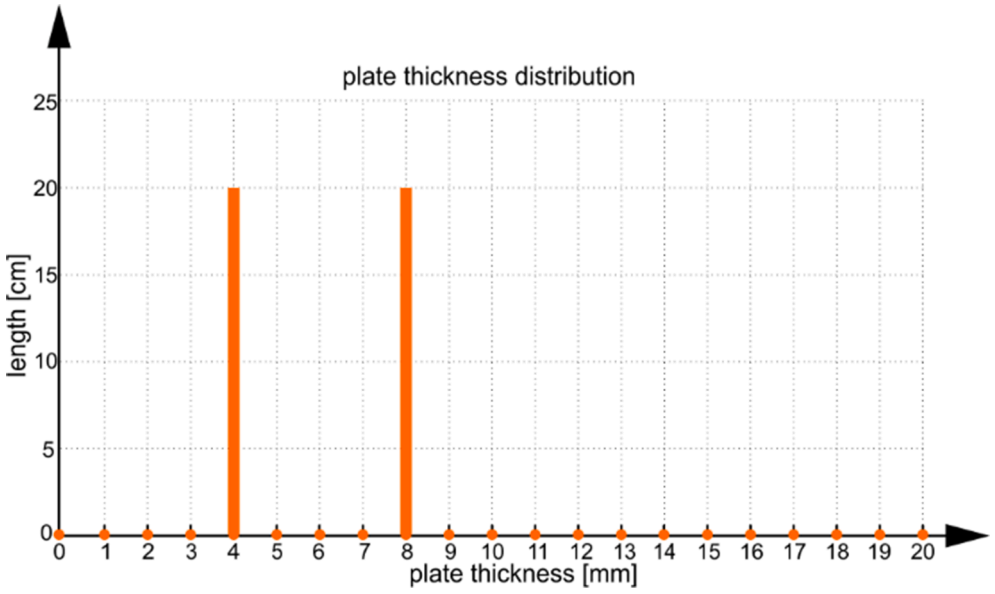

Fig. 8. Numerically obtained thickness distribution of stepped plate.

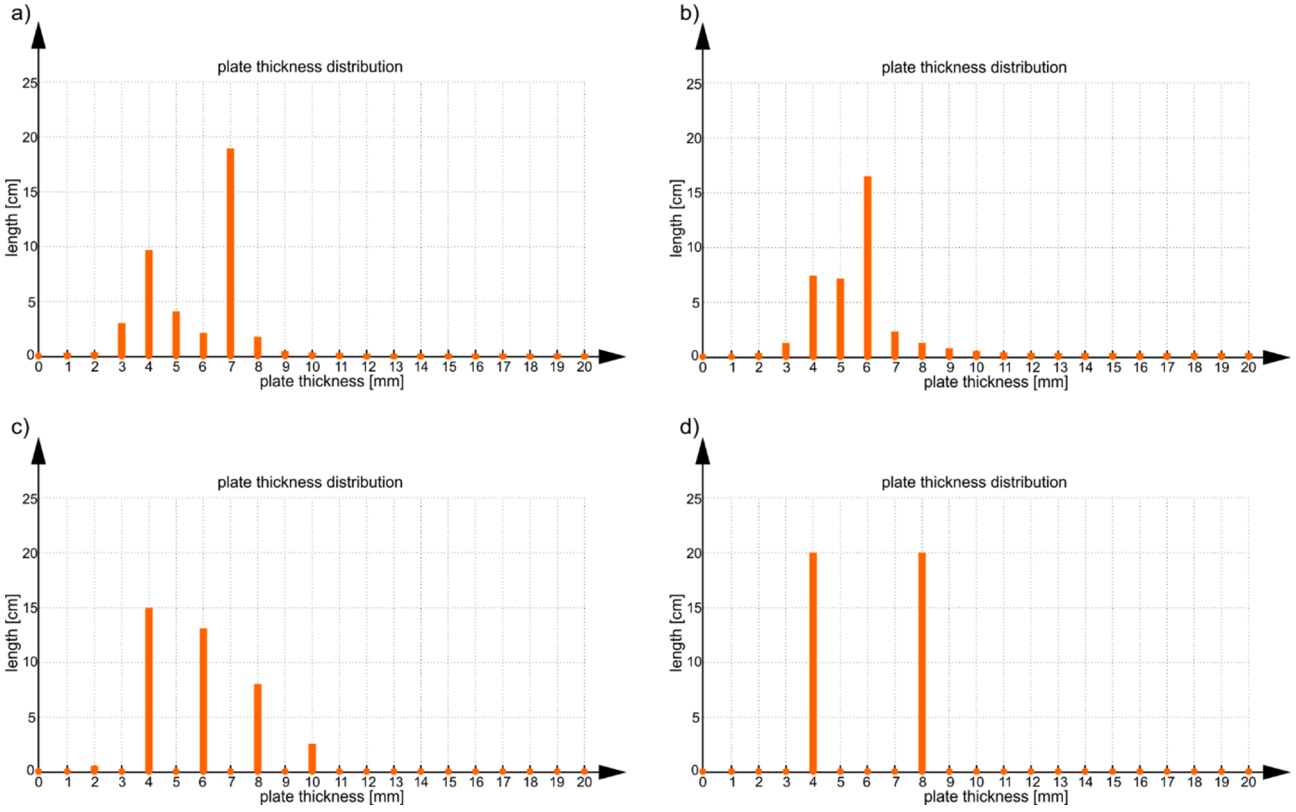

Fig. 9. Numerically obtained thickness distribution of tapered plate for various formulations of dictionary matrix: a) measurements made for frequencies from 50 to 150 kHz with a step of 20 kHz, b) measurements made for frequencies from 50 to 150 kHz with a step of 50 kHz, c) measurements made for a plate thickness from 2 mm to 20 with a step of 2 mm and d) measurements made for a plate thickness from 4 mm to 20 with a step of 4 mm.

5 mm (0.69 cm). The significant length for thickness of 6 mm can be explained by the fact that the average thickness of the considered plates is equal to 6 mm. The minimum plate thickness (4 mm) has also been correctly specified but the corresponding length was underestimated. A similar thickness distribution was obtained also for the limited number of measurements (Fig. 13a). Fig. 13a and Fig. 13b depict the results for a twice and a three times smaller number of measurements, respectively (50–150 kHz with a step of 20 kHz or 30 kHz). The thickness reconstruction made only based on three measurements (Fig. 13b) resulted in the less sparse vector $\mathbf{l}$. It contains the non-zero lengths for thicknesses from 3 to 8 mm, but the lengths corresponding to thicknesses 3, 7, and 8 are negligible and are shorter than 0.5 cm. On the other hand, the possible thickness range was estimated correctly.

The reduction of the dictionary matrix resulted in the detection of

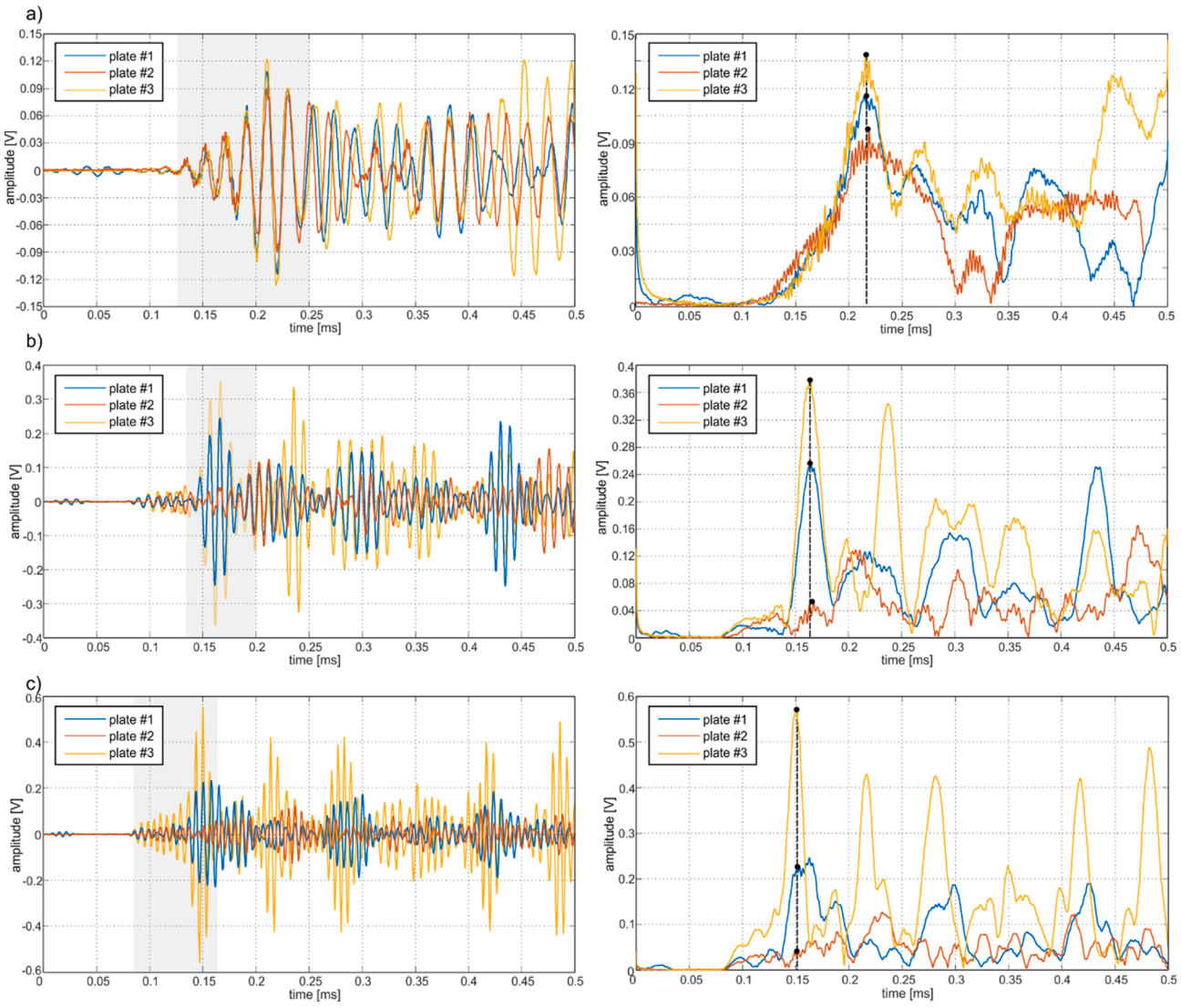

Fig. 10. Experimental signals and their envelopes obtained for plates #1, #2, and 3# for frequency of a) 50 kHz, b) 100 kHz, and c) 150 kHz.

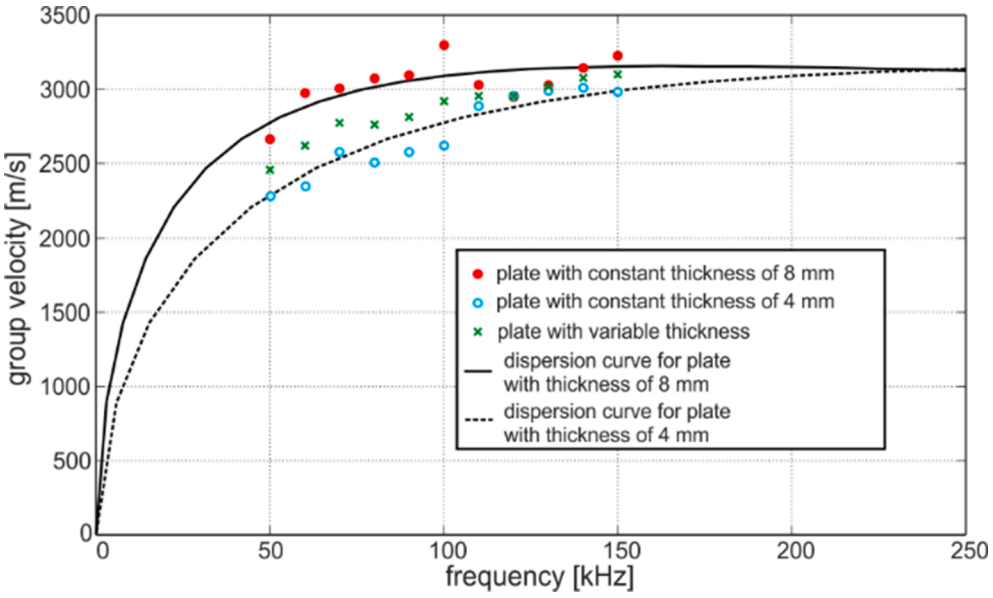

Fig. 11. Experimentally determined group velocities in plates with constant and variable thickness compared with theoretical dispersion curves.

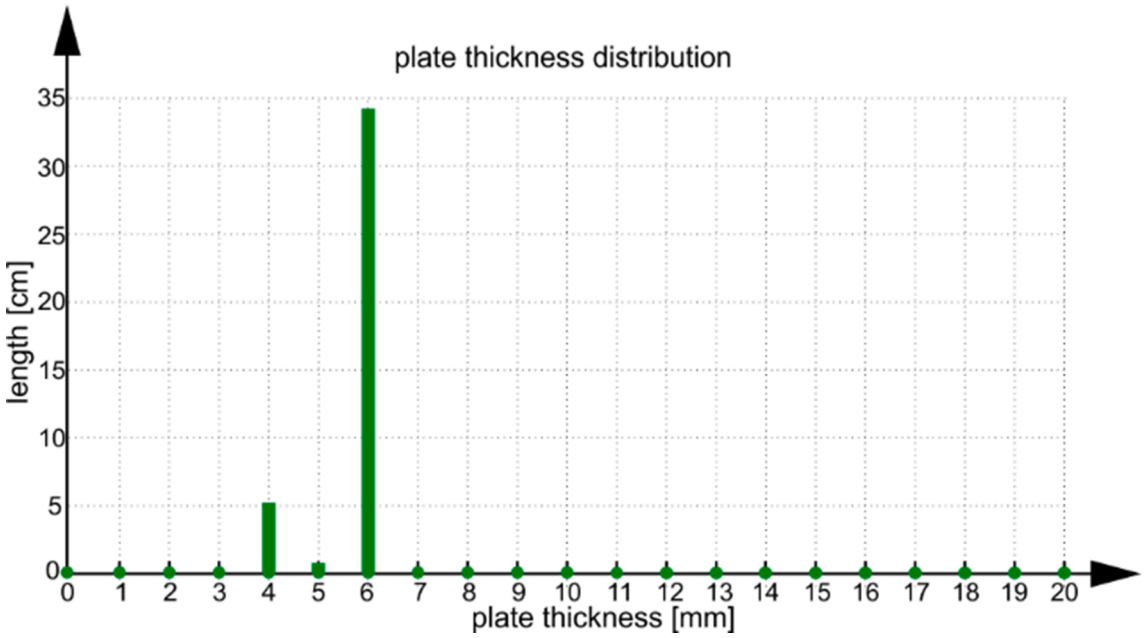

Fig. 12. Experimentally obtained thickness distribution of stepped plate.

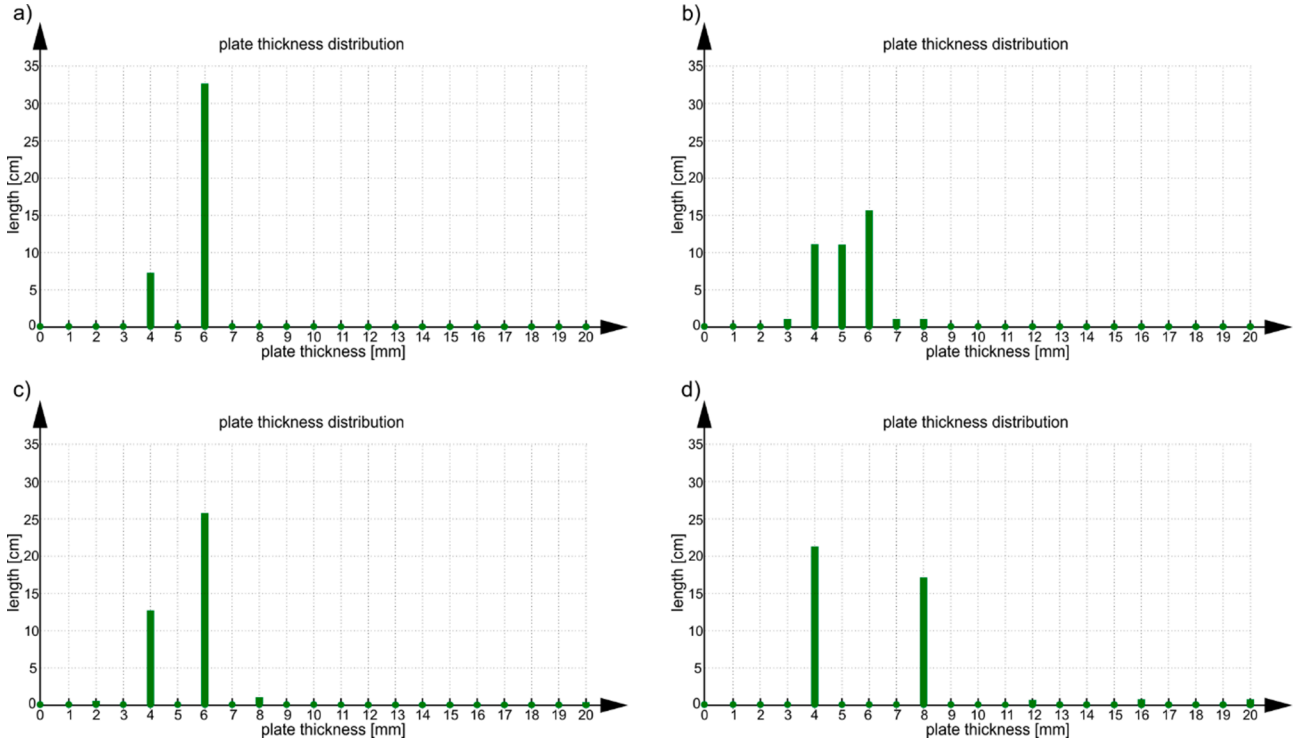

Fig. 13. Experimentally obtained thickness distribution of tapered plate for various formulations of dictionary matrix: a) measurements made for frequencies from 50 to 150 kHz with a step of 20 kHz, b) measurements made for frequencies from 50 to 150 kHz with a step of 50 kHz, c) measurements made for a plate thickness from 2 mm to 20 with a step of 2 mm and d) measurements made for a plate thickness from 4 mm to 20 with a step of 4 mm.

two major thicknesses. Fig. 13c presents the vector **l** determined using an analytical dictionary matrix built for plate thickness varied from 2 mm to 20 mm with a step 2 mm. As in the case of numerical results presented in the previous section the distribution in Fig. 13d reflects best the actual model shape but the dictionary matrix was built only for five thicknesses (4, 8, 12, 16 and 20 mm) and the sparse representation of vector **l** is partly caused by the matrix form.

One can say that in any case, regardless of the size of the dictionary matrix or the number of measurements, the exact thickness distribution was not obtained based on experimental data. However, it must be noted that the inaccuracies in plate thickness reconstruction were mainly caused by the differences between the experimentally determined velocities and analytical velocities, which were used to build the dictionary matrix (Fig. 11). The influence of the discrepancies between experimental and theoretical results is demonstrated in Fig. 14 which presents the thickness distribution obtained by using experimental

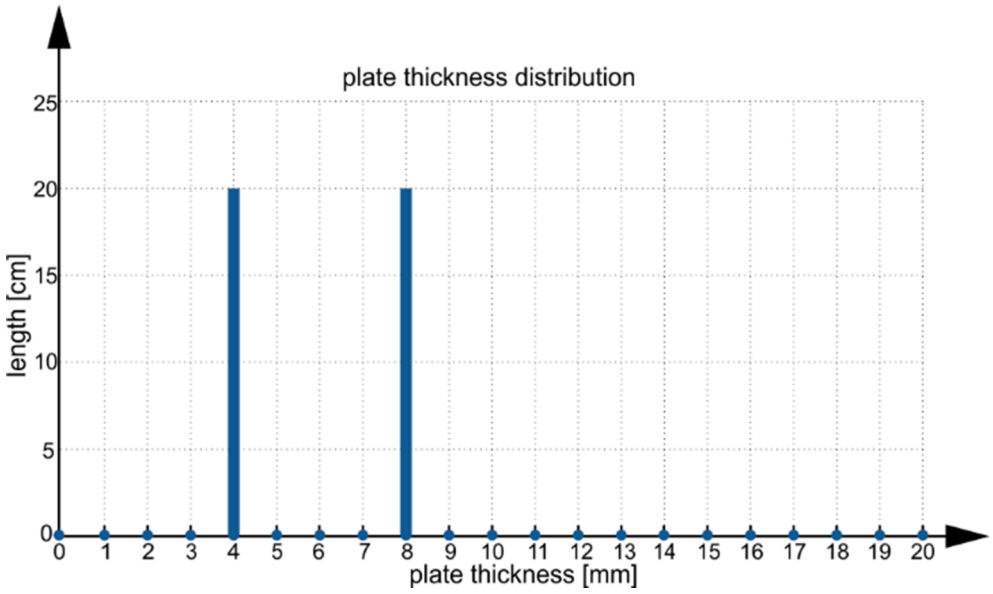

Fig. 14. Experimentally obtained thickness distribution based on modified dictionary matrix built partially on experimental measurements of wave velocity.

measurements but to do this, the dictionary matrix was modified. The theoretically determined reciprocals of velocities for plates with a constant thickness of 4 and 8 mm were replaced with experimental results. For such a case, the plate thickness distribution was determined perfectly.

This analysis unambiguously proved that the proposed approach is correct and efficient but the results strongly depend on the dictionary matrix (its size and the kind of data used to build it).

6. Discussion and conclusions

In this study, the inherent dispersive properties of guided waves were used to propose a novel approach for plate thickness distribution determination. The analysis of the possibility of using a compressed sensing approach in thickness variability assessment was proceeded by analytical analysis resulting in important conclusions.

First of all, it was proved that wave velocity as well as the time course of the incident wave propagating alongside the plate with variable thickness do not depend on the exact shape of this plate, but only on the thickness distribution. On the other hand the other parameter – amplitude – strongly depends on the plate shape and plates with exactly the same thickness distribution may be characterized by significantly different wave amplitude. These findings are crucial in the context of the further development of diagnostics methods aimed at i.e. corrosion degradation assessment. Based on the obtained results we can notice that wave propagates with the same velocity and has the same shape in the two specimens characterized by the same thickness distribution and thus, the same degradation level and mass loss. These parameters may be used in the assessment of total thickness reduction or thickness distribution but they cannot be used for the reconstruction of the exact plate shape. The dependency of wave velocity and thickness distribution was used to propose a novel approach based on constrained convex optimization to determine the plate thickness variability. Both, numerical and experimental results unambiguously proved that the convex-based method allows, among others, to estimate the minimal thickness of the plate, which is particularly important in the context of structural strength and load capacity. However, because of the insensitivity of wave velocity on plate shape, it is impossible to indicate where exactly the cross-section with minimal thickness is localized.

On the other hand, the third considered parameter i.e. amplitude demonstrated high sensitivity to plate shape and thus we can conclude that the potential damage indexed dedicated to e.g. corrosion assessment should not be based solely on the amplitude variability, especially in the case of non-constant monitoring. In the future perspective, the exact plate shape reconstruction the advantage of both, amplitude, velocity or wave shape should be taken into account.

Ethical statement

Author states that the research was conducted according to ethical standards.

CRediT authorship contribution statement

Beata Zima: Conceptualization, Methodology, Software, Validation, Formal analysis, Investigation, Writing – original draft, Writing – review & editing, Visualization, Supervision, Project administration, Funding acquisition.

Declaration of Competing Interest

The authors declare that they have no known competing financial interests or personal relationships that could have appeared to influence the work reported in this paper.

Acknowledgments

The author greatly acknowledges the support of the Foundation for Polish Science (FNP). The financial support of these studies from Gdańsk University of Technology by the DEC-04/2021/IDUB/II.1/AMERICUM ‘Excellence Initiative - Research University’program is gratefully acknowledged.

References

[1] Z. Su, L. Ye, Y.e. Lu, Guided Lamb waves for identification of damage in composite structures: a review, J. Sound Vib. 295 (3-5) (2006) 753–780.
[2] A. Raghavan, C.E.S. Cesnik, Review of guided wave structural health monitoring, Shock Vib. Digest 39 (2) (2007) 91–114.
[3] M. Mitra, S. Gopalakrishnan, Guided wave based structural health monitoring: a review, Smart Mater. Struct. 25 (5) (2016) 27.
[4] T. Wandowski, P. Malinowski, W. Ostachowicz, Damage detection with concentrated configurations of piezoelectric transducers, Smart Mater. Struct. 20 (2011), 025002 (14 pp).

[5] M. Radzieński, Ł. Doliński, M. Krawczuk, M. Palacz, Damage localization in a stiffened plate structure using a propagating wave, Mech. Syst. Sig. Process. 39 (2013) 388–395.
[6] M. Bahador, A. Zaimbashi, R. Rahgozar, Three-stage Lamb-wave-based damage localization algorithm in plate-like structures for structural health monitoring applications, Signal Process. 168 (2020), 107360.
[7] N. Mori, S. Biwa, T. Kusaka, Damage localization method for plates based on the time reversal of the mode-converted Lamb waves, Ultrasonics 91 (2019) 19–29.
[8] B. Zima, Damage detection in plates based on Lamb wavefront shape reconstruction, Measurement 177 (2021) 109206, https://doi.org/10.1016/j.measurement.2021.109206.
[9] L. Maio et al., "Detection of ice accretions on composite panels using FMCW radars at 60GHz," 2021 IEEE 8th International Workshop on Metrology for AeroSpace (MetroAeroSpace), 2021, pp. 636-639, doi: 10.1109/MetroAeroSpace51421.2021.9511775.
[10] S. Shoja, V. Berbyuk, A. Boström, Guided wave-based approach for ice detection on wind turbine blades, Wind Eng (2018).
[11] Q.-T. Deng, Z.-C. Yang, Propagation of guided waves in bonded composite structures with tapered adhesive layer, Appl. Math. Modell. 35 (2011) 5369–5381.
[12] N. Bochud, Q. Vallet, J.G. Minonzio, P. Laugier, Predicting bone strength with ultrasonic guided waves, Sci Rep. 3 (7) (2017 Mar) 43628, https://doi.org/10.1038/srep43628. PMID: 28256568; PMCID: PMC5335564.
[13] V. Pagneux, A. Maurel, Lamb wave propagation in elastic waveguides with variable thickness, Proc. R. Soc. London, Ser. A 462 (2006) 1315–1339.
[14] M.-C. El-Kettani, F. Luppé, A. Guillet, Guided waves in a plate with linearly varying thickness: experimental and numerical results, Ultrasonics 42 (1-9) (2004) 807–812.
[15] Nurmalia, N. Nakamura, H. Ogi, M. Hirao, K. Nakahata, Nakahata, Mode conversion behavior of SH guided wave in a tapered plate, NDT and E Int. 45 (1) (2012) 156–161.
[16] L. De Marchi, A. Marzani, N. Speciale, E. Viola, Prediction of pulse dispersion in tapered waveguides, NDT and E Int. 43 (3) (2010) 265–271.
[17] L. De Marchi, A. Marzani, M. Miniaci, A dispersion compensation procedure to extend pulse-echo defects location to irregular waveguides, NDT and E Int. 54 (2013) 115–122.
[18] L. Moreau, J.G. Minonzio, M. Talmant, P. Laugier, Measuring the wavenumber of guided modes in waveguides with linearly varying thickness, J Acoust Soc Am. 135 (5) (2014 May) 2614–2624, https://doi.org/10.1121/1.4869691. Erratum. In: J Acoust Soc Am. 2014 Aug; 136(2):945. PMID: 24815245.
[19] J. Moll, T. Wandowski, P. Malinowski, M.S. Radzienski Opoka, W. Ostachowicz, Experimental analysis and prediction of antisymmetric wave motion in a tapered anisotropic waveguide, J. Acoust. Soc. Am. 138 (2015) 299–306.
[20] J. Moll, Damage localization in composite structures with smoothly varying thickness based on the fundamental antisymmetric adiabatic wave mode, Ultrasonics 71 (2016) 111–114.
[21] A. Martínez, A. Güemes, J.M. Perales, J.M. Vega, Variable Thickness in Plates—A Solution for SHM Based on the Topological Derivative, Sensors. 20 (9) (2020) 2529, https://doi.org/10.3390/s20092529.
[22] H. Lamb, On waves in an elastic plate, Proc. R Soc. London Ser. A, Contain Pap. a Math. Phys. Character. 93 (1917) 114–128.
[23] B. Zima, R. Kędra, Detection and size estimation of a crack in plate based on guided wave propagation Mech, Syst. Signal Proc. 142 (2020), 106788.
[24] Thanasis, Sparse Approximate Solutions to Linear Systems, Siam J. Comput. 24 (1995) 227–234.
[25] E.J. Candes, J. Romberg, T. Tao, Robust uncertainty principles: exact signal reconstruction from highly incomplete frequency information, IEEE Trans. Inform. Theory 52 (2) (2006) 489–509.
[26] D. Alleyne, P. Cawley, A two-dimensional Fourier transform method for the measurement of propagating multimode signals, J. Acoust. Soc. Am. 89 (1991) 1159–1168.
[27] B. Zima, R. Kędra, Numerical study of concrete mesostructure effect on lamb wave propagation, Materials 13 (11) (2020) 2570, https://doi.org/10.3390/ma13112570.